Hole Transport Materials with Low Glass Transition Temperatures and High Solubility for Application in Solid-State Dye-Sensitized Solar Cells

Tomas Leijtens,[†] I-Kang Ding,[‡] Tommaso Giovenzana,[‡] Jason T. Bloking,[‡] Michael D. McGehee,[‡] and Alan Sellinger[‡,*]

[†]Department of Chemical Engineering, Stanford University, Stanford, California 94305, United States, and [‡]Department of Materials Science and Engineering, Stanford University, Stanford, California 94305, United States

ABSTRACT

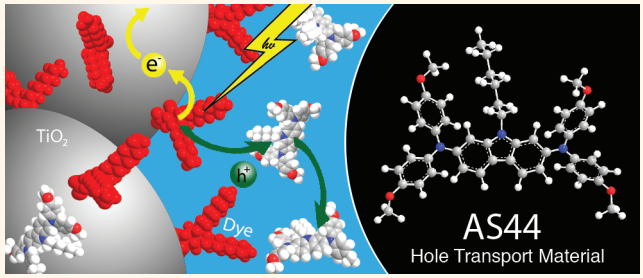

We present the synthesis and device characterization of new hole transport materials (HTMs) for application in solid-state dye-sensitized solar cells (ssDSSCs). In addition to possessing electrical properties well suited for ssDSSCs, these new HTMs have low glass transition temperatures, low melting points, and high solubility, which make them promising candidates for increased pore filling into mesoporous titania films. Using standard device fabrication methods and Z907 as the sensitizing dye, power conversion efficiencies (PCE) of 2.94% in 2-μm-thick cells were achieved, rivaling the PCE obtained by control devices using the state-of-the-art HTM spiro-OMeTAD. In 6-μm-thick cells, the device performance is shown to be higher than that obtained using spiro-OMeTAD, making these new HTMs promising for preparing high-efficiency ssDSSCs.

KEYWORDS: organic photovoltaics · solid-state dye-sensitized solar cells · organic hole transport materials

Dye-sensitized solar cells (DSSCs) have become a promising alternative photovoltaic technology to conventional solar cells since the original report in 1991 by O'Regan and Gratzel.[1] In DSSCs, incoming light is absorbed by a sensitizing dye that is chemically attached to an n-type nanocrystalline titania framework. Upon light excitation, dye molecules inject electrons into the conduction band of the titania network. This is followed by dye regeneration and subsequent hole transport through the hole transport materials (HTM) to the respective electrode. The highest performing DSSCs to date utilize a liquid-based I^-/I_3^- redox couple to regenerate the dye and provide an efficient mechanism for hole transport. However, such cells suffer from potential leakage problems associated with the corrosive and volatile nature of the liquid electrolyte and, thus, may be impractical for large-scale applications.[2] More importantly, the overpotential required for dye regeneration by the I^-/I_3^- redox couple limits the maximum obtainable voltage of the system.[3] In an effort to address these issues, solid-state HTMs with optimized HOMO levels have been the focus of many recent reports. To date, the best performance in such solid-state DSSCs (ssDSSCs) is based on the HTM termed 2,2′,7,7′-tetrakis(*N*,*N*-di-*p*-methoxyphenylamine)-9,9′-spirobifluorene (spiro-OMeTAD)[4] with efficiencies up to 6.1% using custom-synthesized dyes.[5]

Currently, optimized ssDSSCs are limited by insufficient pore filling of the HTMs into thick mesoporous titania films (>5 μm).[6] This insufficient pore filling is due to the method in which the pores are filled. The pore filling procedure begins by spin-coating a solution of the HTM in chlorobenzene onto the dye-sensitized titania film. The wet overlayer of solution on top of the titania film functions as a reservoir, so that as solvent evaporates and the solution concentration increases, HTM diffuses into the pores, allowing for a higher degree of pore filling than would be obtained from the initial concentration of the solution alone. The diffusion stops when either the concentration in the reservoir has increased

* Address correspondence to aselli@stanford.edu.

Received for review November 6, 2011 and accepted January 9, 2012.

Published online January 09, 2012
10.1021/nn204296b

© 2012 American Chemical Society

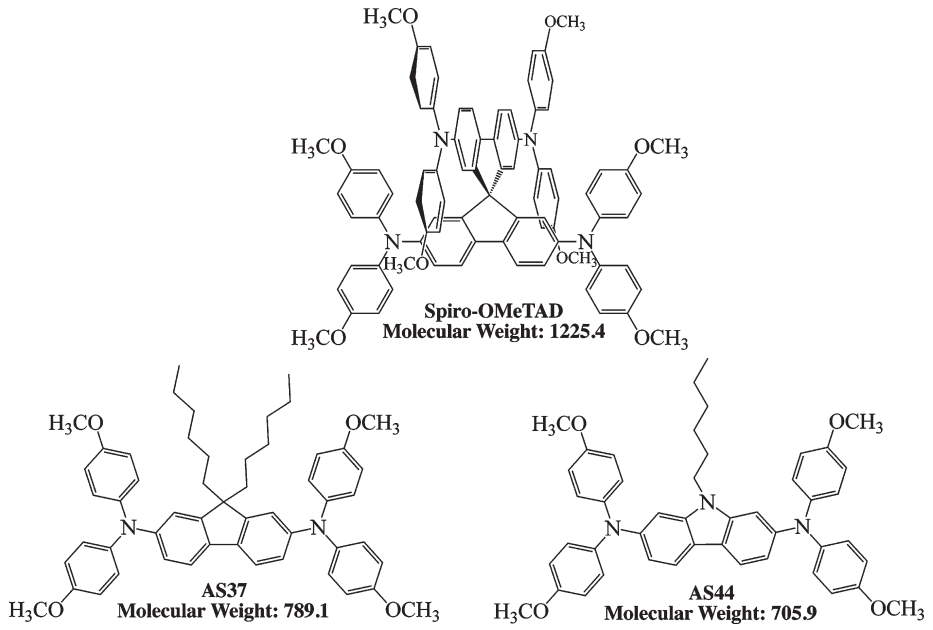

Figure 1. State-of-the-art HTM spiro-OMeTAD and the novel HTMs described in this work, AS37 and AS44.

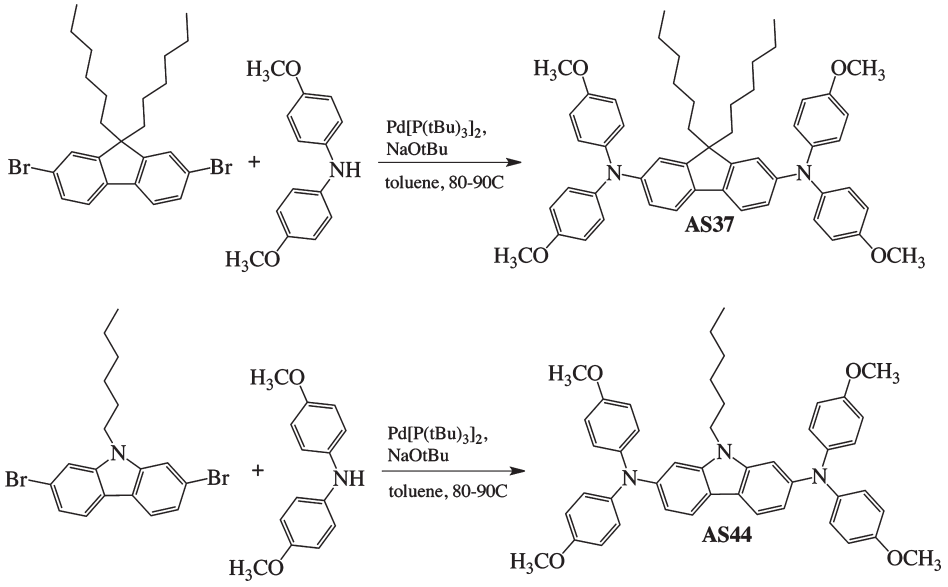

Scheme 1. Synthetic scheme for the preparation of the new hole transport materials.

beyond the HTM's solubility or the reservoir is depleted. In the case where the HTM is spiro-OMeTAD, the total pore volume is only partially filled in optimized devices, while the pore filling in thicker devices is even lower, accelerating the electron−hole recombination and lowering the charge collection efficiency.[6−10] As a result, optimized active layers are only 2−3 μm thick, far thinner than the thickness needed to achieve the desired optical absorption for most commercial sensitizing dyes.

Two potential routes to increase the pore filling and enable the use of thicker ssDSSCs are to use HTMs with higher solubility and/or lower glass transition temperatures for a *melt infiltration* process. Spiro-OMeTAD has a moderate solubility limit in chlorobenzene of about 30 vol %,[10] a glass transition temperature (T_g) of 125 °C, and melting point (T_m) of 248 °C, which lies far above the degradation temperature of most dyes.[11] As a result, attempts to melt infiltrate spiro-OMeTAD have led to poor device performance, likely due to dye degradation.[11,12,22] New materials are therefore required for the successful melt infiltration of solid-state HTMs to enable enhanced pore filling and thicker optimized cells. Such a concept has been demonstrated recently, but the solar cell performances remain unsatisfactory, possibly because the temperatures used (255 °C) still exceeded common degradation temperatures of dyes and the HTM may not have been optimized for use in

TABLE 1. Summary of the Electrochemical, Photophysical, and Thermal Properties of the HTMs Used in This Study

HTM	HOMO (eV)[a,b]	LUMO (eV)[c]	$E_{opt.\ gap}$ (eV)[d]	UV (nm)	T_g (°C)[e]	T_m (°C)[e]
spiro-OMeTAD	−5.11[a] (−5.03)[b]	−2.05	2.98	309, 389(max)	125	248
AS37	−5.14[a] (−4.98)[b]	−1.99	2.99	314, 388(max)	43	106
AS44	−4.98[a] (−4.89)[b]	−1.93	2.96	393	59	132

[a] Determined by photoelectron spectroscopy in air (PESA) of thin films. [b] Determined by solution-based cyclic voltammetry (CV). [c] LUMO = HOMO + $E_{opt.gap}$. [d] Determined at the UV absorption onset. [e] Determined by differential scanning calorimetry (DSC).

ssDSSCs.[12] More recent studies have used liquid thiophene-based monomers to fill the pores followed by photo- and electropolymerization;[13,14] however, this method requires special processing procedures that may be difficult to realize in high-throughput production processes.

Here we report the systematic and straightforward synthesis of two HTM materials that were used to prepare ssDSSC devices by standard processing procedures. The new HTMs were designed to have similar functional groups and energy levels to spiro-OMeTAD yet differ in molecular size, solubility, glass transition temperature, and melting point. One of the HTMs (AS44) produced device performances similar (η = 2.3% average, 2.9% peak) to those of the spiro-OMeTAD devices (η = 2.8% average, 3.4% peak) when using the standard amphiphilic ruthenium sensitizing dye, Z907.[15] To the best of our knowledge, these power conversion efficiencies (PCE) values are among the highest reported to date for small-molecule HTMs other than spiro-OMeTAD.[16−21] Moreover, even without the introduction of a melt infiltration process, thick cells (6 μm) made with AS44 perform better (η = 2.3%) than those made with spiro-OMeTAD (η = 2.1%), which we propose is due to the new materials' high solubility (and therefore enhanced pore filling in thick cells). With these highly soluble and low-T_g HTMs, PCEs can be achieved that rival spiro-OMeTAD in thin (2 μm) cells, outperform spiro-OMeTAD in thick (>5 μm) cells, and have the potential to use melt infiltration to reach even higher PCEs in the future

RESULTS AND DISCUSSION

Materials Synthesis and Characterization. The materials design rationale was to prepare HTMs with high solubility and low glass/melting transition temperatures while systematically examining the basic components of the state-of-the-art HTM, spiro-OMeTAD. The first step was to look at the importance of the "spiro" structure. For this we designed AS37, where the spiro link was replaced by two hexyl chains. We also replaced the central 2,7-fluorene core with a more electron donating *N*-hexyl-2,7-carbazole core (AS44). The synthetic procedure to prepare the materials is shown in Scheme 1. The preparation was straightforward, *i.e.*, linking readily available starting precursors using palladium-catalyzed Buchwald−Hartwig aminations to provide the desired materials in >70% yield after purification by column chromatography. The materials purity was determined by ^{1}H/^{13}C NMR, size exclusion chromatography (SEC), matrix-assisted laser desorption/ionization time of flight spectrometry (MALDI-TOF), and thermal properties by differential scanning calorimetry (DSC). DSC results (Table 1) show that replacing the spiro linkage of spiro-OMeTAD with two hexyl groups (AS37) substantially reduces the T_g and T_m to 43° and 106 °C, respectively, while replacing the central fluorene core with *N*-hexyl-2,7-disubstituted carbazole (AS44) results in a T_g and T_m respectively of 59° and 132 °C.

TABLE 2. Conductivity and Mobility Levels of the Materials Used in This Study[a]

	conductivity (S cm^{-1})	mobility (cm^2 V^{-1} s^{-1})
Spiro	2×10^{-5}	4×10^{-5}
Spiro (Sb)	2×10^{-5}	2×10^{-5}
AS37	4×10^{-6}	5×10^{-5}
AS37 (Sb)	6×10^{-6}	1×10^{-4}
AS44	7×10^{-7}	1×10^{-5}
AS44 (Sb)	2×10^{-5}	1×10^{-5}

[a] Doped materials are denoted with (Sb).

The highest occupied molecular orbital (HOMO) level energies of the HTMs were determined on thin films using photoelectron spectroscopy in air (PESA) and dilute solutions using cyclic voltammetry (CV) and are reported in Table 1. Films were deposited on glass substrates by spin-coating solutions with HTM concentrations of 50 mg mL^{-1} in chlorobenzene to yield ∼100 nm thick films. Since HOMO levels vary only ±0.1 eV from spiro-OMeTAD, hole injection from the dye to the HTM should be similar. HOMO values from CV analysis were also very similar to spiro-OMeTAD. It also should be noted that the increased donor character of the carbazole core in AS44 does result in a slight increase of the HOMO from both PESA (−4.98 eV) and CV (−4.89 eV) measurements over spiro-OMeTAD and AS37. After hole injection, the holes must be efficiently transported to the cathode. For this reason, the hole mobility values were measured by using the space charge limited current (SCLC) method. Devices for measuring the mobility were prepared following a published procedure.[23] These samples all contained the *tert*-butyl pyridine (TBP) and lithium bis(trifluoromethylsulfonyl)imide salt (Li-TFSI) additives in the concentrations that yielded the best solar cells to ensure that the mobilities obtained corresponded to those found in solar cells. In the case where the contacts are ohmic and any trap states filled, the current density *J* is limited by space charge and is given

by the expression

$$J(V) = \frac{9\varepsilon\varepsilon_0\mu V^2}{8d^3} \quad (1)$$

where ε is the dielectric constant of the material (normally taken to approach 3 for organic semiconductors),[24] μ is the hole mobility, V is the applied bias, and d is the film thickness. Fitting the $J-V$ curves for each material to this expression gives the mobilities listed in Table 2. This method has been shown to be applicable to many organic semiconductors, including spiro-OMeTAD.[23,24] The plots used to calculate the mobilities are included in the Supporting Information.

The value obtained here for spiro-OMeTAD treated with TBP and Li-TFSI is slightly lower, but similar to that reported in the literature.[23,24] The mobilities of AS37 and AS44, p-doped and undoped, are very close to that of spiro-OMeTAD obtained in this study. The dopant used in this study was tris(4-bromophenyl)aminium hexachloroantimonate (TBPA) at levels of 0.36 mol %, and these samples are denoted throughout this section of the article by (Sb).

We note that AS37 (Sb) demonstrates a higher hole mobility than spiro-OMeTAD and is the only HTM that showed a significant increase in hole mobility upon p-doping. It has been shown that p-doping over 1 mol % is necessary to increase the mobility of spiro-OMeTAD. Only then are the coulomb traps caused by the dopant anions offset by a reduction in barrier height to charge hopping.[24] The latter is due to overlapping of the associated coulomb wells. In the case of AS37 however, this point seems to be reached at lower dopant concentrations, as the mobility is shown to increase substantially upon 0.36 mol % doping.

The conductivities of the films were measured using four-point probe methodology. The same additives as those used for the mobility measurements were applied here. The electrodes had a high width to length ratio and were closely spaced. Here, width is the dimension perpendicular to the current flow, so these electrodes were very wide compared to the length of the measured device. This limited the edge effects, making the conduction path linear. Results are given in Table 2, and the conductivity of spiro-OMeTAD closely matches that reported in the literature[24] of 10^{-5} S cm^{-1}.

The conductivity of doped AS44 is very similar to that of spiro-OMeTAD, while that of AS37 (doped and undoped) is 3 times lower. There does not seem to be a clear trend with regard to the effects of p-doping of the HTM. Still, it is evident that doping AS44 results in a significant increase in conductivity, while doping AS37 results in an increase in mobility so that both of the doped materials' electrical properties are very similar to those of spiro-OMeTAD. Hence, one would expect the hole transport through the HTM in the ssDSSC to be very similar to that of spiro-OMeTAD. It is also interesting to note that even though the HOMO level of AS44 is roughly 100 meV higher than that of spiro-OMeTAD (−4.98 *vs* −5.08 eV), it still needs to be doped with TBPA to increase its conductivity. This may indicate that, unlike spiro-OMeTAD, AS44 is not doped by ambient oxygen, a desired property for reproducibility and preparation of devices in inert atmospheres.

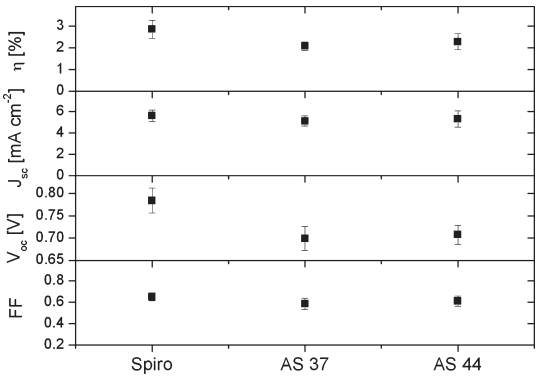

Figure 2. Graphical representations of ssDSSCs devices using the various HTMs. (a) Power conversion efficiency, (b) short-circuit current, (c) open-circuit voltage, and (d) fill factor, where the error bars stand for the standard deviation in the data. Spiro-OMeTAD is included as a reference and denoted as spiro. All the AS materials are doped with 0.36 mol % TPBA. TPBA does not improve the performance of spiro-based devices.

It has been shown that the electron conductivity and mobility in mesoporous titania are significantly lower than the conductivity and hole mobility of spiro-OMeTAD.[25,26] It is then proposed that hole transport through the HTM is not the primary limiting factor in device performance. In the case of AS44 (Sb) and AS37 (Sb), the conductivity and mobility values fall within the range such that hole transport should be similar to that in spiro-OMeTAD and should not limit the device performance. In the case of spiro-OMeTAD, it is proposed that the recombination at the dye−HTM interface and pore filling in thick devices limits device performance.[6,10,25,28,30] As AS44 (Sb) and AS37 (Sb) have similar charge transport properties to spiro-OMeTAD, and assuming similar recombination kinetics to spiro-OMeTAD due to the similarity in chemical structures and HOMO levels, we expect PCEs to be similar in thin cells that do not suffer from low pore filling. The potential for improved pore filling in thick cells due to the HTM's higher solubility could result in improved performance in thick devices as compared to spiro-OMeTAD.

Device Performance of 2-μm-thick ss-DSSCs. ss-DSSCs were fabricated according to a slight modification to reported procedures (see Methods),[8,27] with the commercially available dye Z907 used as the sensitizing dye. We note also that all devices were prepared with optimized final overlayer thicknesses (50−300 nm, confirmed by cross sectional SEM). The mean device parameters for 2 μm devices are given in Figure 2. The synthesized HTMs perform remarkably well, but only upon p-doping. For

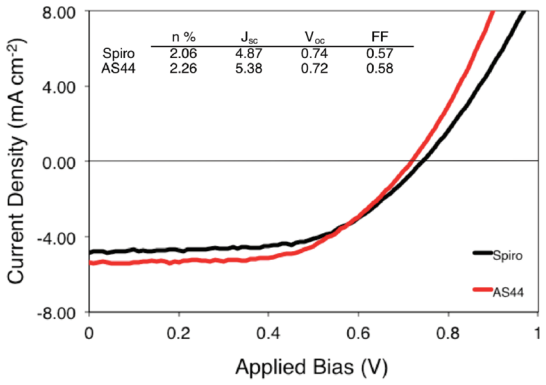

Figure 3. *J*–*V* curves of 6 μm ss-DSSCs made with spiro-OMeTAD (black line) and AS44 (red line). The inset provides numerical values for the device characteristics.

example, without TPBA doping the AS37- and AS44-based devices achieved PCEs of 1.5% and 0.5%, respectively. When doped, AS37 (Sb) and AS44 (Sb) perform particularly well with regard to the J_{sc} and FF, to yield mean overall efficiencies of 2.0% and 2.3% with best device performances reaching 2.48% and 2.94%, respectively.

The V_{oc}'s of AS37 (Sb) and AS44 (Sb) are very similar, but are 100 mV lower than that of spiro-OMeTAD. This could be due to their HOMO levels being slightly higher than that of spiro-OMeTAD. It is also possible that these materials, because of their smaller molecular size than spiro-OMeTAD, can more easily approach the titania interface to lower V_{oc} due to an increase in electron–hole recombination at the titania interface, lowering the quasi-Fermi level of titania. FF and J_{sc} of AS37 (Sb) and AS44 (Sb) are slightly lower but comparable to those of spiro-OMeTAD. This is expected because these materials have charge transport properties similar to spiro-OMeTAD and, therefore, will have high enough conductivity and mobility values so that they are not limiting charge transport.[24–26]

Device Performance of 6-μm-thick ss-DSSCs. Due to the increased solubility of the new HTMs coupled with the promising results in 2-μm-thick cells, we performed preliminary studies in 6-μm-thick cells. We chose to use only AS44 for this preliminary measurement, as it displayed better performance than AS37 in 2-μm-thick cells. The preliminary results are promising, with AS44 outperforming spiro-OMeTAD.

The *J*–*V* curves (Figure 3) show that cells made with spiro-OMeTAD suffer significantly from the increase in thickness ($\eta = 2.1\%$), whereas the cells made from AS44 seem to perform equally well ($\eta = 2.3\%$) as those made with 2 μm cells. The low performance of spiro-OMeTAD corresponds to the low degree of pore filling previously reported in thick titania films[7] and, as predicted by Melas-Kyriazi *et al.*,[7] suffers most from an average decrease in V_{oc} from 0.80 to 0.74 V. The decrease in pore filling likely results in injected holes recombining more frequently at the titania–HTM interface since these charges must travel within a thin coating of HTM in close proximity to the titania.[7,10] This subsequently lowers the quasi-fermi level of titania, decreasing the V_{oc}. The J_{sc} has also dropped significantly (from 5.6 to 4.9 mA cm^{-2}) because the low degree of pore filling prevents the oxidized dye molecules from being efficiently regenerated, and more charge carriers are lost through increased recombination, leading to a loss in overall charge generation. The performance of AS44 in thicker devices, while better than that of spiro-OMeTAD, does not exceed that observed at 2 μm, reaching an efficiency of 2.3%. Notably, the V_{oc} of the thick AS44 devices is not decreased from its value in thin devices, suggesting that there is no recombination-induced voltage drop in the titania electron quasi-fermi level. This allows us to propose that while the titania–HTM recombination is increased in spiro-OMeTAD-based devices as the thickness is increased, the recombination in AS44-based devices is relatively unaffected by the increasing thickness.

We believe that the high solubility of the new materials should result in significantly improved pore filling in thick devices, as would be suggested by the above discussion of device performance and the relative V_{oc}'s.[7] As both AS37 and AS44 have much higher solubility than spiro-OMeTAD, much higher solution concentrations can be used during application of the HTM by spin coating. The importance of their high solubility is explained in the pore filling mechanism verified by Ding *et al.*[6] The diffusion of HTM from the reservoir in the wet overlayer should be able to continue until the concentration of HTM in the reservoir is much higher than that possible in the case of spiro-OMeTAD, so that more HTM is diffused into the pores to give a higher PFF. Note that in order to maintain reasonable final HTM overlayer thicknesses (50–300 nm) in our ssDSSCs, we used spin-coating concentrations of 500 mg mL^{-1} for AS37 and AS44, much higher than the 360 mg mL^{-1} used for spiro-OMeTAD. This may be an indication that more of the HTM is diffusing into the pores rather than drying on top of the substrate.

The device results are promising, but leave room for improvement, as one would ideally hope to observe an improved current at such a device thickness due to an increase in light absorption. We propose that the pore filling in the cells made from AS44, while likely higher than that of spiro-OMeTAD due to the increased solubility, may still need to be improved by the introduction of a melt infiltration process to enable more efficient dye regeneration and transport before increased charge generation and higher currents are realized. With this in mind, we expect that optimization using better sensitizing dyes, together with the introduction of a heating step at temperatures above the T_g, should increase pore filling further and lead to even better performance in the future. We note that such a melt infiltration process is not currently feasible with spiro-OMeTAD, so that the materials presented here offer a significant advantage. This work is currently in progress and will be published in the near future.

CONCLUSIONS

In conclusion, two new HTMs for application in ssDSSC have been synthesized and characterized. The electronic properties of the materials are similar to those of the current state-of-the-art HTM, spiro-OMeTAD, and this is reflected in their promising photovoltaic performances. Moreover, likely due to higher solubility, preliminary data demonstrate superior performance of one of the new HTMs (AS44) in thicker ss-DSSCs (6 μm) compared to spiro-OMeTAD. Further improvements are expected with optimization and attempts at melt infiltration, which should be possible due to the materials' low T_g's. These novel, highly performing materials then offer a unique opportunity to achieve efficient ssDSSCs at thickness levels above 5 μm.

METHODS

Materials Characterization. All materials were purchased from Sigma-Aldrich, TCI America, and Strem Chemicals and used as received. 2,7-Dibromocarbazole was provided as a gift from St. Jean Photochemicals (http://www.sjpc.com/). ^{1}H and ^{13}C NMR spectra were recorded using a Varian Inova 400 or 500 in d_6-DMSO or benzene (C_6D_6) at 298 K. Differential scanning calorimetry analyses were performed on a DSC Q100 (TA Instruments). DSC curves were recorded at a scanning rate of 10 °C/min under nitrogen flow. UV−vis absorption spectra were recorded in a UV−vis spectrophotometer (Cary 6000i) at room temperature using a glass cuvette with a path length of 1 cm. Matrix-Assisted Laser Desorption/Ionization Time-of-Flight Mass Spectrometry (MALDI-TOF MS) was performed on an Applied Biosystems TF4800 MALDI-TOF-Mass Spectrometer using reflection positive mode. Samples were prepared at a concentration of 10 mg/ml in THF and α-cyano-4-hydroxycinnamic acid (2 mg/ml in THF) was used as the matrix.

Cyclic voltammetry measurements[29] were carried out on a CHI411 electrochemical workstation, using a concentration of a few mM in dichloromethane containing approximately 0.05 M supporting electrolyte of tetrabutylammoniun hexafluorophosphate, $Bu_4N^+PF_6^-$, in a three-electrode cell, where the saturated calomel electrode was used as the reference electrode and platinum wire as the working electrode. The scanning rate was 100 mV s^{-1}. Photoelectron spectra in air were recorded on a Riken Keiki AC-2 ultraviolet photoelectron spectrophotometer.

Experimental Procedure for *N*-Hexyl-2,7-dibromocarbazole. 2,7-Dibromocarbazole (730 mg, 2.25 mmol) and sodium *tert*-butoxide (283 mg, 2.94 mmol) were transferred to a 50 mL Schlenk flask and connected to a Schlenk line. The flask was subjected to three vacuum/nitrogen refill cycles in order to remove water and oxygen. Anhydrous DMF was added (15 mL) followed by 1-iodohexane (0.5 mL, 3.29 mmol), and the mixture was stirred for 4 h at 130 °C or until the reaction was complete by thin layer chromatography (TLC) analysis. The product was isolated by the addition of DI-water and EtOAc and extracted with further DI-water, followed by a brine solution. The EtOAc layer was dried over $MgSO_4$, filtered, and concentrated by a rotary evaporator. The collected crude solids were purified by column chromatography (hexane/EtOAc, 9.5:0.5) to afford a white solid. Final yield: 92%.

^{1}H NMR (DMSO, 400 MHz, 298 K): δ 8.11 (d, 2H, J = 8.41 Hz), 7.88 (s, 2H), 7.34 (d, 2H, J = 8.41 Hz), 4.37 (t, 2H, J = 6.62 Hz), 1.68 (t, 2H, J = 6.58 Hz), 1.24 (m, 6H), 0.80 (t, 3H, J = 7.09 Hz)

Experimental Procedure for AS44. *N*-Hexyl-2,7-dibromocarbazole (548 mg, 1.34 mmol), bis(4-methoxyphenyl)amine (629 mg, 2.74 mmol), sodium *tert*-butoxide (321 mg, 3.34 mmol), bis(dibenzylidenacetone)palladium(0) ($Pd(dba)_2$) (28.8 mg, 0.05 mmol), and 1,1′-bis(diphenylphosphino)ferrocene (dppf) (27.7 mg, 0.05 mmol) were transferred to a 50 mL Schlenk flask and connected to a Schlenk line. The flask was subjected to three vacuum/nitrogen refill cycles in order to remove water and oxygen. Anhydrous toluene was added (15 mL), and the mixture was stirred for 12 h at 110 °C or until the reaction was complete by TLC analysis. The product was collected by extraction with addition of EtOAc and DI-water (3×), followed by a brine solution (1×). The toluene/EtOAc layer was dried with $MgSO_4$, filtered, and concentrated by a rotary evaporator. The collected crude solids were purified by column chromatography (hexane/EtOAc, 9:1) to give a pale yellow solid. Final yield: 74%.

^{1}H NMR (DMSO, 400 MHz, 298 K): δ 7.73 (d, 2H, J = 8.41 Hz), 6.97 (m, 8H), 6.85 (m, 10H), 6.65 (dd, 2H, J = 8.39 Hz), 3.86 (t, 2H, J = 6.62 Hz), 3.71 (s, 12H), 1.45 (t, 2H, J = 6.58 Hz), 1.04 (m, 6H), 0.74 (t, 3H, J = 7.09 Hz). ^{13}C NMR (C_6D_6, 100 MHz, 298 K): δ 155.88, 146.99, 142.50, 126.11, 120.46, 118.55, 115.72, 114.96, 102.96, 54.91, 42.40, 31.66, 26.78, 24.31, 22.63, 14.11. MALDI TOF MS: *m/z* 705.19, calc 705.36.

Experimental Procedure for AS37. 9,9′-Dihexyl-2,7-dibromofluorene (722 mg, 1.47 mmol), bis(4-methoxyphenyl)amine (739 mg, 3.23 mmol), sodium *tert*-butoxide (423 mg, 4.41 mmol), bis(dibenzylidenacetone)palladium(0) ($Pd(dba)_2$) (34.5 mg, 0.06 mmol), and 1,1′-bis(diphenylphosphino)ferrocene (dppf) (33.2 mg, 0.06 mmol) were transferred to a 50 mL Schlenk flask and connected to a Schlenk line. The flask was subjected to three vacuum/nitrogen refill cycles in order to remove water and oxygen. Anhydrous toluene was added (15 mL), and the mixture was stirred for 12 h at 110 °C or until the reaction was complete by TLC analysis. The product was collected by extraction with addition of EtOAc and DI-water (3×), followed by a brine solution (1×). The toluene/EtOAc layer was dried with $MgSO_4$, filtered, and concentrated by a rotary evaporator. The collected crude solids were purified by column chromatography (hexane/EtOAc, 9:1) to give a pale yellow solid. Final yield: 78%.

^{1}H NMR (DMSO, 400 MHz, 298 K): δ 7.45 (d, 2H, J = 8.22 Hz), 6.95 (m, 8H,), 6.86 (m, 10H), 6.73 (dd, 2H, J = 8.18 Hz), 3.72 (s, 12H), 1.64 (t, 4H, J = 7.55 Hz), 1.11 (m, 4H), 1.01 (m, 8H), 0.77 (t, 6H, J = 7.13 Hz), 0.58 (m, 4H). ^{13}C NMR (C_6D_6, 100 MHz, 298 K): δ 156.04, 152.17, 147.85, 142.08, 135.53, 126.26, 121.22, 119.87, 116.97, 114.97, 55.13, 54.89, 40.41, 31.84, 30.01, 24.31, 22.29, 14.25.

ss-DSSC Procedure. Samples for ss-DSSC performance were prepared according to the standard procedure.[8] Briefly, fluorine-doped tin oxide substrates (15 Ω cm^{-1}, Pilkington) were etched with zinc powder and HCl (4 M) to give the desired electrode patterning. These substrates were coated with a compact TiO_2 layer (50 nm) by aerosol spray pyrolysis deposition at 450 °C using air as the carrier gas. TiO_2 films of 2 μm were then deposited on the substrates by doctor-blading TiO_2 from a commercial paste (Dyesol 18NR-T) and slowly heating the substrates to 500 °C to bake for 30 min in air. For the 6 μm TiO_2 films, three layers of paste were deposited by doctor-blading, and samples were heated to 125 °C for 10 min between layers. The samples were then immersed into an acidic 0.02 M aqueous $TiCl_4$ solution overnight at room temperature, followed by heating to 450 °C. After cooling to 80 °C, the substrates were immersed in a 0.3 mM Z907 dye solution (Solaronix SA in a 1:1 mixture of acetonitrile and *tert*-butyl alcohol) overnight followed by rinsing with acetonitrile. The dye had been purified by column chromatography using Sephadex LH20 and methanol as eluent. The formulation of the spiro-OMeTAD solution used for spin-coating on 2-μm-thick devices has been published elsewhere.[8] The solutions for spin-coating the hole transport materials followed this formulation with the following exceptions: the concentration of AS44 in chlorobenzene was 240 mg mL^{-1} instead of the normal 225 mg mL^{-1}, the *tert*-butylpyridine to HTM (for AS37, AS44) ratio was 1:17.3 μL mg^{-1}, and the ratio of lithium bis(trifluoromethylsulfonyl)imide salt (170 mg mL^{-1} in acetonitrile)

to HTM (A37, AS44) was 1:8 μL mg^{-1}. The same solution compositions were used for the 6 μm films but with concentrations of 360 and 500 mg mL^{-1} for spiro-OMeTAD and the new HTMs, respectively. Aliquots of the solutions (35 μL) were deposited on 3 cm^2 films of TiO_2 and spun at 2000 rpm for 45 s in air. Back contacts were applied by thermal evaporation of 200 nm of silver. For photovoltaic measurements, an AM 1.5 solar simulator equipped with a Xe lamp was calibrated using a reference Si photodiode equipped with an IR cutoff filter to reduce mismatch in the 350−750 nm region between simulated and AM 1.5 light to below 2%. *I*−*V* curves were taken using a Keithley 2400 source meter.

Mobility Measurements. A hole injecting layer of PEDOT-PSS (25 nm) was applied on pre-etched indium tin oxide substrates by spin-coating. A film of HTM (280 nm), with tbp and Li-TFSI added as described for devices, was then deposited on top of the PEDOT-PSS layer, also by spin-coating. Selected devices were doped by the addition of tris(4-bromophenyl)aminium hexachloroantimonate at levels of 0.36 mol %, and these samples are denoted using (Sb). Silver back electrodes were deposited by thermal evaporation, and *I*−*V* curves taken with a Keitheley 2400 source meter.

Conductivity Measurements. Glass substrates were cleaned by sonication in 10% Extran solution, acetone, and isopropyl alcohol. A thin layer of compact TiO_2 (25 nm) was deposited by aerosol spray pyrolysis at 450 °C.[8] This layer was added to improve the wetting of the HTMs on the substrate. Solutions identical to those used for the mobility measurements were used to spin coat films of HTMs (280 nm thick). Finally, silver electrodes (200 nm) with a high length to width ratio were deposited by thermal evaporation in a vacuum. A four-point probe setup was used with a Keithley 2400 source meter to measure linear *I*−*V* curves.

Acknowledgment. This work was supported by the Office of Naval Research (ONR) through grant N000141110244. MALDI-TOF characterization was performed as part of a User project at the Molecular Foundry, which is funded by the DOE under Contract No.DE-AC02-05CH11231. The authors thank Mr. Cody Montana Sam for his contribution to the TOC figure. A.S. thanks St. Jean Photochemicals (http://www.sjpc.com/) for providing 2,7-dibromocarbazole as one of the starting precursors for AS44.

Supporting Information Available: Characterization of the new materials (^{1}H NMR, ^{13}C NMR, DSC, UV−vis, charge mobility, conductivity, cyclic voltammograms, and PESA results). This material is available free of charge *via* the Internet at http://pubs.acs.org.

REFERENCES AND NOTES

1. O'Regan, B.; Grätzel, M. A Low-Cost, High-Efficiency Solar Cell Based on Dye-Sensitized Colloidal TiO_2 Films. *Nature* **1991**, *353*, 737–740.
2. Kroon, J. M.; Bakker, N. J.; Smit, H. J. P.; Liska, P.; Thampi, K. R.; Wang, P.; Zakeeruddin, S. M.; Grätzel, M.; Hinsch, A.; Hore, S.; *et al*. Nanocrystalline Dye-Sensitized Solar Cells Having Maximum Performance. *Prog. Photovolt: Res. Appl.* **2007**, *15*, 1–18.
3. Snaith, H. J. Estimating the Maximum Attainable Efficiency in Dye-Sensitized Solar Cells. *Adv. Funct. Mater.* **2010**, *20*, 13–19.
4. Bach, U.; Lupo, D.; Comte, P.; Moser, J. E.; Weissortel, F.; Salbeck, J.; Spreitzer, H.; Grätzel, M. Solid-State Dye-Sensitized Mesoporous TiO_2 Solar Cells with High Photon-to-Electron Conversion Efficiencies. *Nature* **1998**, *395*, 583–585.
5. Cai, N.; Moon, S.-J.; Cevey-Ha, N.-L.; Moehl, T.; Humphry-Baker, R.; Wang, P.; Zakeeruddin, S. M.; Grätzel, M. An Organic D-π-A Dye for Record Efficiency Solid-State Sensitized Heterojunction Solar Cells. *Nano Lett.* **2011**, *11*, 1452–1456.
6. Ding, I. K.; Tétreault, N.; Brillet, J.; Hardin, B. E.; Smith, E. H.; Rosenthal, S. J.; Sauvage, F.; Grätzel, M.; McGehee, M. D. Pore-Filling of Spiro-OMeTAD in Solid-State Dye Sensitized Solar Cells: Quantification, Mechanism, and Consequences for Device Performance. *Adv. Funct. Mater.* **2009**, *19*, 2431–2436.
7. Melas-Kyriazi, J.; Ding, I. K.; Marchioro, A.; Punzi, A.; Hardin, B. E.; Burkhard, G. F.; Tétreault, N.; Grätzel, M.; Moser, J.-E.; McGehee, M. D. The Effect of Hole Transport Material Pore Filling on Photovoltaic Performance in Solid-State Dye-Sensitized Solar Cells. *Adv. Energy Mater.* **2011**, *1*, 407–414.
8. Ding, I. K.; Melas-Kyriazi, J.; Cevey-Ha, N.-L.; Chittibabu, K. G.; Zakeeruddin, S. M.; Grätzel, M.; McGehee, M. D. Deposition of Hole-Transport Materials in Solid-State Dye-Sensitized Solar Cells by Doctor-Blading. *Org. Electron.* **2010**, *11*, 1217–1222.
9. Jennings, J. R.; Peter, L. M. A Reappraisal of the Electron Diffusion Length in Solid-State Dye-Sensitized Solar Cells. *J. Phys. Chem. C* **2007**, *111*, 16100–16104.
10. Snaith, H. J.; Humphry-Baker, R.; Chen, P.; Cesar, I.; Zakeeruddin, S. M.; Grätzel, M. Charge Collection and Pore Filling in Solid-State Dye-Sensitized Solar Cells. *Nanotechnology* **2008**, *19*, 424003.
11. Fredin, K.; Anderson, K. F.; Duffy, N. W.; Wilson, G. J.; Fell, C. J.; Hagberg, D. P.; Sun, L.; Bach, U.; Lindquist, S.-E. Effect on Cell Efficiency following Thermal Degradation of Dye-Sensitized Mesoporous Electrodes Using N719 and D5 Sensitizers. *J. Phys. Chem. C* **2009**, *113*, 18902–18906.
12. Fredin, K.; Johansson, E. M. J.; Blom, T.; Hedlund, M.; Plogmaker, S.; Siegbahn, H.; Leifer, K.; Rensmo, H. Using a Molten Organic Conducting Material to Infiltrate a Nanoporous Semiconductor Film and Its Use in Solid-State Dye-Sensitized Solar Cells. *Synth. Met.* **2009**, *159*, 166–170.
13. Zhang, W.; Cheng, Y.; Yin, X.; Liu, B. Solid-State Dye-Sensitized Solar Cells with Conjugated Polymers as Hole-Transporting Materials. *Macromol. Chem. Phys.* **2011**, *212*, 15–23.
14. Liu, X.; Zhang, W.; Uchida, S.; Cai, L.; Liu, B.; Ramakrishna, S. An Efficient Organic-Dye-Sensitized Solar Cell with *in Situ* Polymerized Poly(3,4-ethylenedioxythiophene) as a Hole-Transporting Material. *Adv. Mater.* **2010**, *22*, E150–E155.
15. Zakeeruddin, S. M.; Nazeeruddin, M. K.; Humphry-Baker, R.; Pechy, P.; Quagliotto, P.; Barolo, C.; Viscardi, G.; Grätzel, M. Design, Synthesis, and Application of Amphiphilic Ruthenium Polypyridyl Photosensitizers in Solar Cells Based on Nanocrystalline TiO_2 Films. *Langmuir* **2002**, *18*, 952–954.
16. Kroeze, J. E.; Hirata, N.; Schmidt-Mende, L.; Orizu, C.; Ogier, S. D.; Carr, K.; Grätzel, M.; Durrant, J. R. Parameters Influencing Charge Separation in Solid-State Dye-Sensitized Solar Cells Using Novel Hole Conductors. *Adv. Funct. Mater.* **2006**, *16*, 1832–1838.
17. Li, B.; Wang, L.; Kang, B.; Wang, P.; Qiu, Y. Review of Recent Progress in Solid-State Dye-Sensitized Solar Cells. *Sol. Energy Mater. Sol. Cells* **2006**, *90*, 549–573.
18. Yanagida, S.; Yu, Y.; Manseki, K. Iodine/Iodide-Free Dye-Sensitized Solar Cells. *Acc. Chem. Res.* **2009**, *42*, 1827–1838.
19. Snaith, H. J.; Zakeeruddin, S. M.; Wang, Q.; Pechy, P.; Grätzel, M. Dye-Sensitized Solar Cells Incorporating a "Liquid" Hole-Transporting Material. *Nano Lett.* **2006**, *6*, 2000–2003.
20. Zhao, Y.; Chen, W.; Zhai, J.; Sheng, X.; He, Q.; Wei, T.; Bai, F.; Jiang, L.; Zhu, D. Solid-State Dye-Sensitized Photovoltaic Device with Newly Designed Small Organic Molecule as Hole-Conductor. *Chem. Phys. Lett.* **2007**, *445*, 259–264.
21. Johansson, E. M. J.; Karlsson, P. G.; Hedlund, M.; Ryan, D.; Siegbahn, H.; Rensmo, H. K. Photovoltaic and Interfacial Properties of Heterojunctions Containing Dye-Sensitized Dense TiO_2 and Tri-arylamine Derivatives. *Chem. Mater.* **2007**, *19*, 2071–2078.
22. Tuyet Nguyen, P.; Degn, R.; Thai Nguyen, H.; Lund, T. Thiocyanate Ligand Substitution Kinetics of the Solar Cell Dye Z-907 by 3-Methoxypropionitrile and 4-tert-Butylpyridine at Elevated Temperatures. *Sol. Energy Mater. Sol. Cells* **2009**, *93*, 1939–1945.
23. Poplavskyy, D.; Nelson, J. Nondispersive Hole Transport in Amorphous Films of Methoxy-Spirofluorene-Arylamine Organic Compound. *J. Appl. Phys.* **2003**, *93*, 341–346.
24. Snaith, H. J.; Grätzel, M. Enhanced Charge Mobility in a Molecular Hole Transporter via Addition of Redox Inactive Ionic Dopant: Implication to Dye-Sensitized Solar Cells. *Appl. Phys. Lett.* **2006**, *89*, 262114.

25. Snaith, H. J.; Grätzel, M. Electron and Hole Transport through Mesoporous TiO_2 Infiltrated with Spiro-MeOTAD. *Adv. Mater.* **2007**, *19*, 3643–3647.
26. Yanagida, S.; Yu, Y.; Manseki, K. Iodine/Iodide-Free Dye-Sensitized Solar Cells. *Acc. Chem. Res.* **2009**, *42*, 1827–1838.
27. Ding, I.-K.; Zhu, J.; Cai, W.; Moon, S. J.; Cai, N.; Wang, P.; Zakeeruddin, S. M.; Grätzel, M.; Brongersma, M. L.; Cui, Y.; *et al*. Plasmonic Dye-Sensitized Solar Cells. *Adv. Energy Mater.* **2011**, *1*, 52–57.
28. Schmidt-Mende, L.; Grätzel, M. TiO_2 Pore-Filling and Its Effect on the Efficiency of Solid-State Dye-Sensitized Solar Cells. *Thin Solid Films* **2006**, *500*, 296–301.
29. Cardona, C. M.; Li, W.; Kaifer, A. E.; Stockdale, D.; Bazan, G. C. Electrochemical Considerations for Determining Absolute Frontier Orbital Energy Levels of Conjugated Polymers for Solar Cell Applications. *Adv. Mater.* **2011**, *23*, 2367–2371.
30. Snaith, H. J.; Moule, A. J.; Klein, C.; Meerholz, K.; Friend, R. H.; Grätzel, M. Efficiency Enhancements in Solid-State Hybrid Solar Cells via Reduced Charge Recombination and Increased Light Capture. *Nano Lett.* **2007**, *7*, 3372–3376.